Macromolecules

pubs.acs.org/Macromolecules Article

Methyl Benzoylformate Derivative Norrish Type I Photoinitiators for Deep-Layer Photocuring under Near-UV or Visible LED

Xianglong He, Yanjing Gao, Jun Nie, and Fang Sun*

Cite This: *Macromolecules* 2021, 54, 3854−3864

Read Online

ACCESS | Metrics & More | Article Recommendations | Supporting Information

ABSTRACT: We designed and prepared a series of methyl benzoylformate (MBF) derivatives Norrish type I photoinitiators (MBFs) for light-emitting diode (LED)-induced photopolymerization through computer simulation. The potential photolysis mechanism of MBFs under LED at 405 nm was explored by steady-state photolysis, nuclear magnetic resonance, and electron spin resonance. The as-synthesized photoinitiator dimethyl 1,4-dibenzoylformate (DM-BD-F) can efficiently initiate free radical photopolymerization of acrylate monomers under LED irradiation at 405 nm. Moreover, we predicted well the photoinitiating capability of MBFs through the cleavage exothermy (ΔH) calculated by triplet bond dissociation energy (BDE) and triplet energy (E_T). Significantly, based on the weak absorption of MBFs at 405 nm, MBFs were successfully applied to deep-layer photocuring and the curing depth reached 6.5 cm after the irradiation of LED at 405 nm for 30 s. This research provides a new idea and efficient strategy for the molecular design of photoinitiators for deep-layer photocuring.

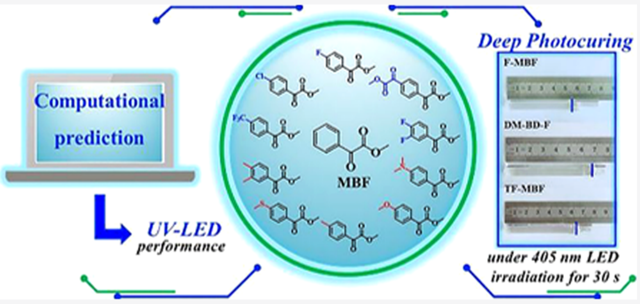

1. INTRODUCTION

Light-emitting diode (LED)-induced photopolymerization technology has prominent advantages compared with traditional photopolymerization technology using high-pressure mercury lamps as light sources because LEDs possess many merits such as long service life, low energy consumption, safety, and environmental protection[1−3] in comparison with high-pressure mercury lamps. However, the main absorption wavelengths of most traditional photoinitiators (PIs) generally are shorter than 365 nm and do not match with the emission wavelengths (usually 385, 395, 405, and 455 nm) of LEDs, which results in the fact that most of the commercially available PIs cannot be used for LED-induced photopolymerization. Therefore, the development of novel PIs used for LED photopolymerization has become the focus of research in recent years.

At present, the reported PIs used for LED-induced photopolymerization are mostly Norrish type II on account of their outstanding absorption in the near-UV and visible-light range and multifunctionality, for example, quinones,[2,4−9] thioxanthones,[10,11] 1,8-naphthalimides,[12−14] curcuminoids,[15,16] and phenothiazines.[17] However, Norrish type II PIs based on hydrogen abstraction mechanism require to form a photoinitiating system together with hydrogen donors or iodonium salts (Iods) to initiate the reaction, which results in the complexity, odor, toxicity, and yellowing of formulations.[18] Conversely, Norrish type I PIs can undergo a direct bond homolytic cleavage to generate reactive radicals to initiate polymerization without any hydrogen donor, which is beneficial for overcoming the disadvantages of Norrish type II. Therefore, the development of Norrish type I PIs used for LED-induced photopolymerization is extremely urgent.[19]

A few Norrish type I PIs including acylphosphine oxides,[20−22] oxime esters,[3,19,23−26] naphthalimide aryl sulfide derivatives,[27,28] and α-dicarbonyls[29−32] for LED-induced photopolymerization have been reported recently. However, they still have some drawbacks. First, the molecules of these reported PIs have large conjugate structures (namely, chromophores) endowing PIs with good absorption capacity in the emission wavelength range of LED, which causes a poor solubility of PIs in monomers and photocured product to be color, thereby seriously limiting the application of PIs in colorless systems. In addition, the large chromophores of the PIs also block deeper light penetration, which leads to the fact that the PIs cannot be applied in thick film curing systems.[25] At present, designing photobleachable PIs is the main way to solve applications of photoinitiators in colorless or deep-layer curing systems.[25,33,34] Li et al.[25] reported a series of photobleachable coumarin-based oxime esters Norrish type I PIs, which showed outstanding photobleaching ability and

Received: December 28, 2020
Revised: February 28, 2021
Published: April 6, 2021

https://doi.org/10.1021/acs.macromol.0c02868

Scheme 1. Chemical Structures of MBFs

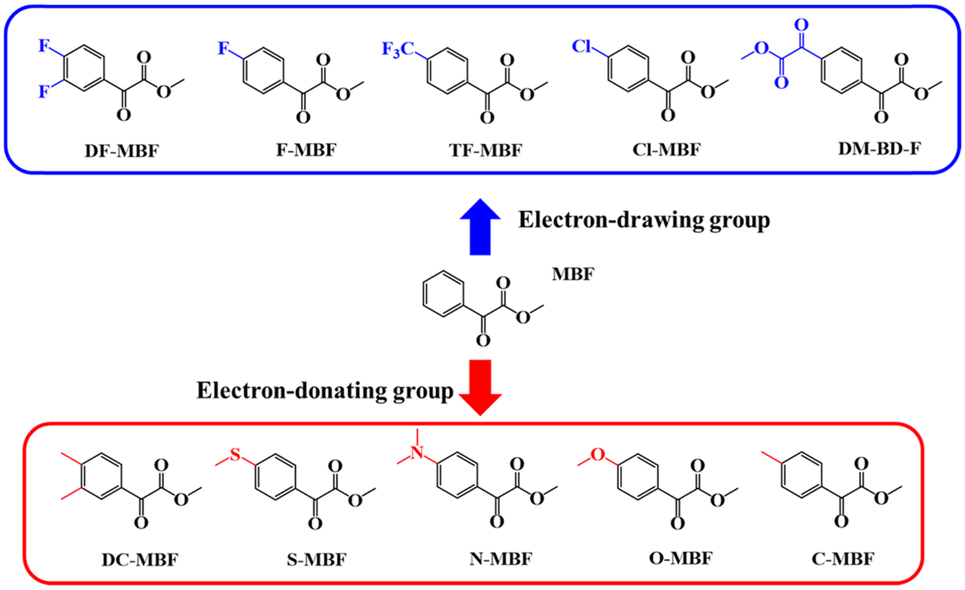

enabled photocuring of thick materials (~4.8 mm) under 455 nm LED. Liska et al.[34] designed a novel acylstannane-based Norrish type I photoinitiator, which had highly initiating activity for radical photopolymerization under above 500 nm LED and presented fast photobleaching both in solution and within the polymer network. Although photobleaching can reduce the yellowing of photocured materials caused by photoinitiators, it is hard for yellow color to disappear thoroughly because the PIs in the photocuring system are hard to decompose down completely, especially for deep-layer curing systems. Moreover, synthesis procedures of these reported PIs with photobleaching capability are cumbersome and demanding, which may greatly restrict their practical application.

In light of the disadvantages of photobleachable photoinitiators, it is imperative and significant to design novel Norrish type I PIs with light color or no color and simple synthesis procedure for colorless or deep-layer photocuring systems under LED irradiation. Methyl benzoylformate (MBF) as a Norrish type I photoinitiator under UV source irradiation was reported because of its good absorption at UV region. It is worth noting that the light-colored MBF has a weak absorption at common LED emission wavelengths (385, 395, 405 nm). The weak absorption is beneficial for light penetration and may endow MBF with good initiation property,[35] which may open up the possibility for MBF derivatives to be used for colorless or deep-layer photocuring systems under LED irradiation. To the best of our knowledge, there is no report on MBF derivatives used for colorless or deep-layer photocuring systems under LED irradiation.

In this work, we designed and synthesized 10 methyl benzoylformate derivatives (MBFs), which have very sample structures as shown in Scheme 1 and can be used for colorless or deep-layer photocuring systems under LED irradiation. Then, we explored the photochemical properties and photolysis mechanism of MBFs through ultraviolet−visible (UV−vis) absorption spectroscopy, electron spin resonance (ESR), and nuclear magnetic resonance (NMR). Photopolymerization kinetics of MBFs/tri (propylene glycol) diacrylate (TPGDA) or trimethylolpropane triacrylate (TMPTA) under LED irradiation at 405 nm was investigated upon real-time infrared spectroscopy (RTIR). Deep curing experiments of MBFs/TPGDA under LED irradiation at 405 nm were carried out. Importantly, we predicted very well the photoinitiating performances of designed MBFs by a computer simulating relevant parameters involving the geometries of ground state and triplet state, energy of triplet state, and cleavage exothermy (ΔH) of PIs before their synthesis, which may provide a significant reference and an effective strategy for research and design on PIs.

2. EXPERIMENTAL SECTION

2.1. Materials. 4-Trifluoromethyl acetophenone was purchased from Heowns Biochem Technologies Ltd. Methyl benzoylformate (MBF), benzyl methyl sulfide, 1-(3,4-difluorophenyl)ethanone, 4′-acetylacetophenone, *N-tert*-butyl-2-phenylnitrone (PBN), dicyclohexylcarbodiimide (DCC), and methyl oxalyl chloride were obtained from Shanghai Bide Pharmatech Ltd. Fluorobenzene, chlorobenzene, toluene, anisole, *o*-xylene, petroleum ether (PE), dichloromethane, ethyl acetate (EA), methanol, anhydrous acetonitrile, pyridine, aluminum trichloride ($AlCl_3$), anhydrous sodium sulfate (Na_2SO_4), and hydrochloric acid were supplied by Beijing Chemical Work (Beijing, China). Dimethylaminobenzene, selenium dioxide, tri(propylene glycol) diacrylate (TPGDA), trimethylolpropane triacrylate (TMPTA), phenylbis (2,4,6-trimethylbenzoyl) phosphine oxide (BAPO), and dibenzoyl (DB) were obtained from Energy Chemical. *tert*-Butylbenzene was purchased from J&K Scientific Ltd. Deuterated chloroform (d_1-$CDCl_3$) and deuterated acetonitrile (d_3-CD_3CN) were supplied by Sinopharm Chemical Reagent Co. Ltd. Molecular structures of commercial PIs and monomers used for experiments are depicted in Scheme 2.

2.2. Characterization. ^1H NMR (400 MHz) and ^{13}C NMR (100 MHz) spectra of MBFs and steady-state photolysis and ^1H NMR (400 MHz) spectra of steady-state photolysis products of S-MBF were recorded by Bruker AV400 unity spectrometer (400 MHz). The high-resolution mass spectra in acetonitrile were acquired with an Agilent 6540 QToF mass detector equipped with an electrospray ionization source. UV−vis absorption properties and steady-state photolysis behaviors of relevant PIs were investigated using a Shimadzu UV-3600 UV−vis−NIR spectrophotometer.

2.3. Irradiation Sources. A Shenzhen Lamplic household LED bulb was used as the irradiation device, the emission wavelength was

Scheme 2. Molecular Structures of Commercial PIs and Monomers Used for Experiments

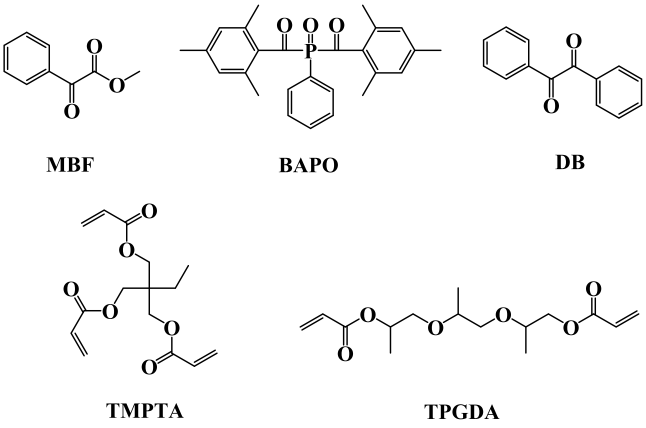

concentrated at 405 and 455 nm, and the intensity of reaching the surface of the photopolymerizable solution was 100 mW cm^{-2}.

2.4. ESR Experiments. Electron spin resonance (ESR) tests of MBFs were operated by a JEOL JES-FA200 spectrometer (X-band) at 9.06 GHz and 100 kHz field modulation, and the microwave power was 0.998 mW. The radicals were generated at room temperature upon LED irradiation at 405 nm under nitrogen atmosphere and next trapped by PBN. MBFs and PBN were dissolved by *tert*-butylbenzene, and concentrations of MBFs were 1×10^{-4} mol L^{-1}. The molar ratio between MBFs and PBN was 1:5. Radicals generated by DB at room temperature under nitrogen atmosphere were trapped by PBN under irradiation of 385 nm LED, the concentration was 1×10^{-4} mol L^{-1}, and the molar ratio between MBFs and PBN was 1:5 also.

2.5. Computational Procedure. The computer calculations of MBFs were calculated by Gaussian 09W package (based on the density functional theory) and utilized Multiwfn and VMD software for drawing and visual analysis. The optimized molecular geometries of the ground state and triplet state of MBFs were obtained by the B3LYP/6-31G(d) level. Bond dissociation energy (BDE) of the ground state and triplet state, triplet-state energy (E_T), and cleavage exothermy (ΔH) of MBFs were gained after frequency calculations which used for determining whether optimized geometries had energy minima. The molecular transition method and frontier molecular orbit were calculated at the TD/B3LYP/6-31G(d) levels.

2.6. Photopolymerization Experiments. The photopolymerization kinetics for photopolymerizable solution consisting of the photoinitiator (BAPO or MBFs) and the monomer (TPGDA or TMPTA) (the mass ratio of photoinitiator to monomer was 1:100) were investigated upon utilizing a Nicolet 5700 FT-IR spectroscope. The photopolymerizable solution was injected into the laminate between two KBr plates (~30 μm) and exposed under LED at 405 nm (~100 mW cm^{-2}). The conversion of the double bond for TPGDA or TMPTA was calculated by comparing the peak areas of 1658−1599 nm^{-1}, and each sample was tested three times.[20]

2.7. Deep-Layer Polymerization Test. The deep polymerization tests were implemented through the following procedure. First, we prepared photopolymerizable TPGDA solutions with a mass fraction of 1% (relative to TPGDA) BAPO, F-MBF, TF-MBF, and DM-BD-F, respectively. Subsequently, the photopolymerizable solutions were injected into four tubes with a depth of 7.5 cm and a diameter of 0.7 cm; then, the tubes with solutions were irradiated from the bottom of tubes by LED with 100 mW cm^{-2} at 405 nm. The distance from the light source to the bottom of the tube was 4 cm. The tubes were turned upside down and the depth of the cured PTPGDA in the tubes was measured after 30 s of irradiation.

2.8. Synthesis of MBFs. The synthesis routes of MBFs are exhibited in Scheme 3. Methyl *p*-fluorobenzoylformate (F-MBF) was synthesized according to the following procedure.[32] Fluorobenzene (0.384 g, 4 mmol) and aluminum trichloride (0.638 g, 4.8 mmol) were dissolved in a flask with 20 mL of dichloromethane and then the flask was moved to an ice-water bath at 0 °C. Methyl oxalyl chloride (0.392 g, 3.2 mmol) was dissolved in 10 mL of dichloromethane and

Scheme 3. Synthesis Routes of MBFs

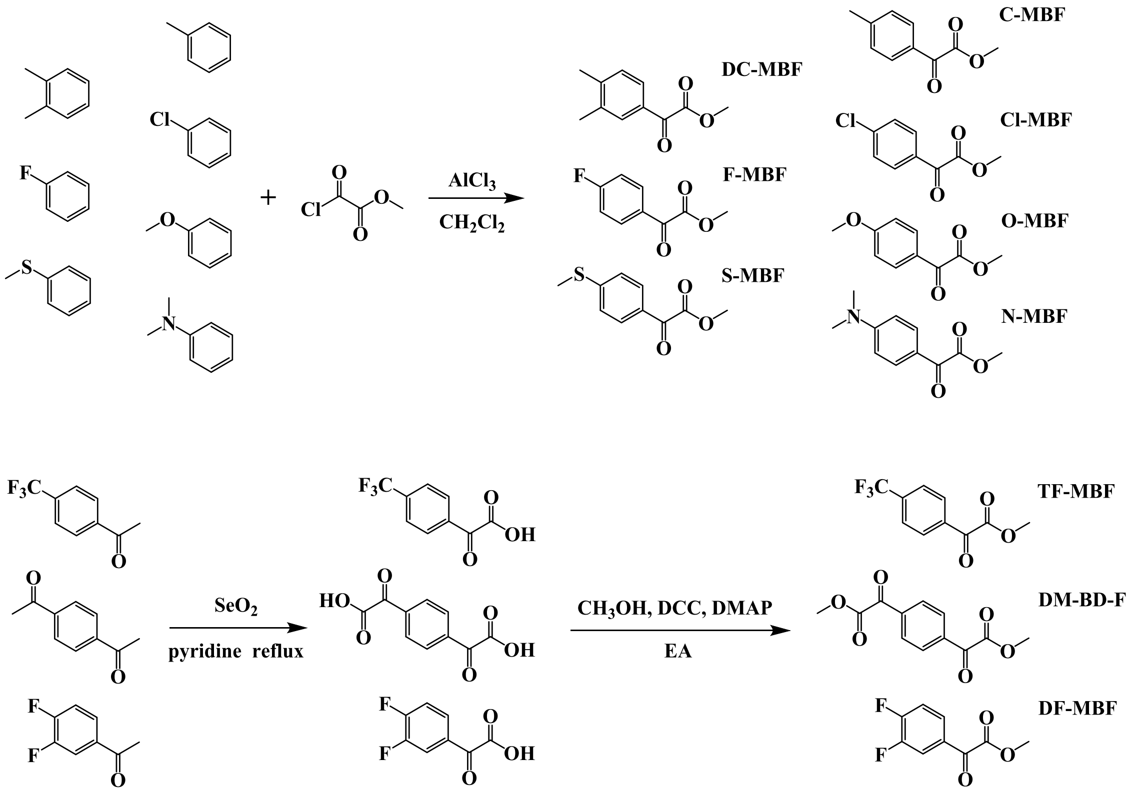

added dropwise (3–4 s per drop) into the flask through a dropping funnel. After the addition, the reaction temperature was increased to 25 °C and the temperature maintained for 4 h, and the progress of the reaction was monitored by thin-layer chromatography (TLC). Subsequently, the reaction solution was poured into 50 mL of ice-water and stirred for 5 min, and the organic layer was separated and collected; then, the aqueous layer was extracted by dichloromethane (3 × 10 mL). The combined organic layer was washed with sodium chloride saturated solution and dried by anhydrous sodium sulfate. The dichloromethane solvent was removed by vacuum distillation and the crude product was purified by silica gel column chromatography (petroleum ether/ethyl acetate = 12/1, volume ratio) to obtain pure F-MBF (cream-colored solid, overall yield 61%). The synthesis methods of S-MBF, C-MBF, Cl-MBF, O-MBF, N-MBF, and DC-MBF are similar to that of F-MBF. Their specific synthesis methods and characterization data are shown in the Supporting Information (Figures S1–S14).

Methyl *p*-trifluoromethylbenzoylformate (TF-MBF) was synthesized according to the following procedure.[36] First, the *p*-trifluoromethyl acetophenone (0.564 g, 3 mmol) and selenium dioxide (SeO_2, 0.501 g, 4.5 mmol) were added to anhydrous pyridine (10 mL) in the flask flushed with nitrogen. The reaction mixture was heated to 110 °C and the temperature maintained for 1 h. Then, the temperature was reduced to 90 °C and kept for an additional 4 h, and the progress of the reaction was monitored by TLC. The solution was filtered using a suction funnel to remove precipitated selenium, and the residue was washed with ethyl acetate (50 mL). The combined filtrate was treated with 20 mL of HCl with a concentration of 1 mol L^{-1} until the pH of the aqueous layer was 3; then, the organic layer was separated and the aqueous layer was extracted with ethyl acetate (5 × 20 mL). Subsequently, organic layers were combined, dried by anhydrous sodium sulfate, and used for the next step of the synthesis.

Next, methanol (0.192 g, 6 mmol), dicyclohexylcarbodiimide (DCC, 0.928 g, 4.5 mmol), and 4-dimethylaminopyridine (DMAP, 0.037 g, 0.3 mmol) were dissolved in a flask with 20 mL of ethyl acetate and stirred at 25 °C; then, the crude solution obtained in the first step was dropped into the reaction flask (1 s per drop) using a dropping funnel. The white precipitate was removed by a suction funnel after the dropping and the organic layer was washed with water. The organic layer was separated and the aqueous layer was extracted with ethyl acetate (3 × 20 mL); then, the organic layers were combined and dried by anhydrous sodium sulfate. The ethyl acetate was removed by vacuum distillation and the crude product was purified by silica gel column chromatography (petroleum ether/ethyl acetate = 12/1, volume ratio) to obtain pure TF-MBF (pale yellow liquid, overall yield 46%). The synthesis methods of DF-MBF and DM-BD-F are similar to that of TF-MBF. Their specific synthesis methods and characterization data are shown in the Supporting Information (Figure S15–S20).

3. RESULTS AND DISCUSSION

3.1. Light Absorption Property.

The UV–vis absorption spectra of MBFs and BAPO in anhydrous acetonitrile are exhibited in Figure 1, and the molar extinction coefficients (ε) of MBFs and BAPO at the maximum absorption wavelength and common LED emission wavelengths (385, 395, 405, and 455 nm) in anhydrous acetonitrile are presented in Table S1. The maximum absorption wavelengths of MBFs all show a red-shift compared with MBF whether the benzene ring of MBFs link electron-withdrawing groups or electron-donating groups expect for TF-MBF. For N-MBF and S-MBF, the introduction of strong electron-donating groups dimethylamino and methylthio causes a significant red-shift of the maximum absorption wavelength and a high molar extinction coefficient (43800 M^{-1} cm^{-1} at 360 nm for N-MBF and 29660 M^{-1} cm^{-1} at 326 nm for S-MBF). However, the absorption wavelength of TF-MBF is blue shifted by more than 9 nm compared with MBF even though the molar extinction coefficient of TF-MBF is greater, which is because the trifluoromethyl group in the TF-MBF molecule is a very strong electron-withdrawing group and cannot be conjugated with the benzene ring. Significantly, N-MBF possesses the most excellent absorption property under the common LED emission wavelengths, followed by the commercial BAPO, and other investigated PIs exhibit lower molar extinction coefficients such as 10 M^{-1} cm^{-1} at 405 nm for MBF and F-MBF, but that does not mean they do not possess photoinitiating ability under LED emission wavelength because the initiating performances of PIs do not depend only on their light absorption properties.[26]

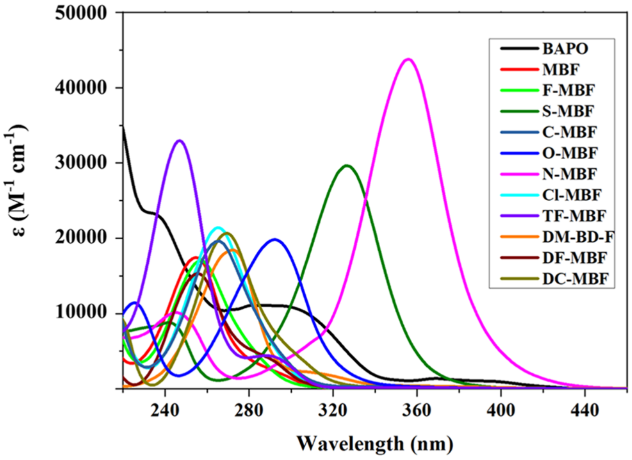

Figure 1. UV–vis absorption spectra of MBFs and BAPO in anhydrous acetonitrile (concentration = 1 × 10^{-4} mol L^{-1}).

Two lowest-energy electronic transitions, transitions type, energy gap of $S_0 \rightarrow S_1$, and the frontier molecular orbits for MBFs are shown in Figures S21–S31 and Table S2. The two lowest-energy transitions of MBFs for $S_0 \rightarrow S_1$ are n–π* transition characteristics or π–π* transition characteristics. In general, PIs with a small energy gap of $S_0 \rightarrow S_1$ have more excellent absorption performance in the visible-light region.[29]

3.2. Photochemistry of MBFs.

The steady-state photolysis curves of MBF, F-MBF, and S-MBF in anhydrous acetonitrile are displayed in Figure 2. Their maximum absorption peaks decline significantly without co-initiator after 120 s of LED irradiation at 405 nm under nitrogen atmosphere, which is key evidence for MBFs as cleavable PIs.[29]

Scheme 4 reveals the types of radicals generated potentially by the cleavage of MBFs under LED irradiation according to the literature.[32] ^{1}H NMR (400 MHz) spectra of the steady-state photolysis products for S-MBF are displayed in Figure 3. Newly generated peaks (*e*, *f*, and *g*) belonging to 4,4′-dimethylthiobenzyl could be apparently seen when S-MBF solution was irradiated for 120 s; at the same time, the peak *h* belonging to dimethyl oxalate was also discovered, demonstrating distinct evidence of the cleavage reaction that occurred in the C–C bond between dicarbonyls.

The ESR spectra of MBFs in the presence of PBN as a trapping reagent under 405 nm LED exposure and the simulations of ESR spectra for MBF, F-MBF, and S-MBF are exhibited in Figures 4 and S32. The hyperfine coupling constant of benzoyl radical (α_N = 14.20 G, α_H = 5.80 G) was obtained by DB upon 385 nm LED exposure for 300 s trapped by PBN in *tert*-butylbenzene (Figure S33a), while the hyperfine coupling constants of the *p*-fluorobenzylbenzoyl radical (α_N = 13.30 G, α_H = 1.60 G), the *p*-methylthiobenzoyl radical (α_N = 14.21 G, α_H = 4.80 G), and the methyl radical

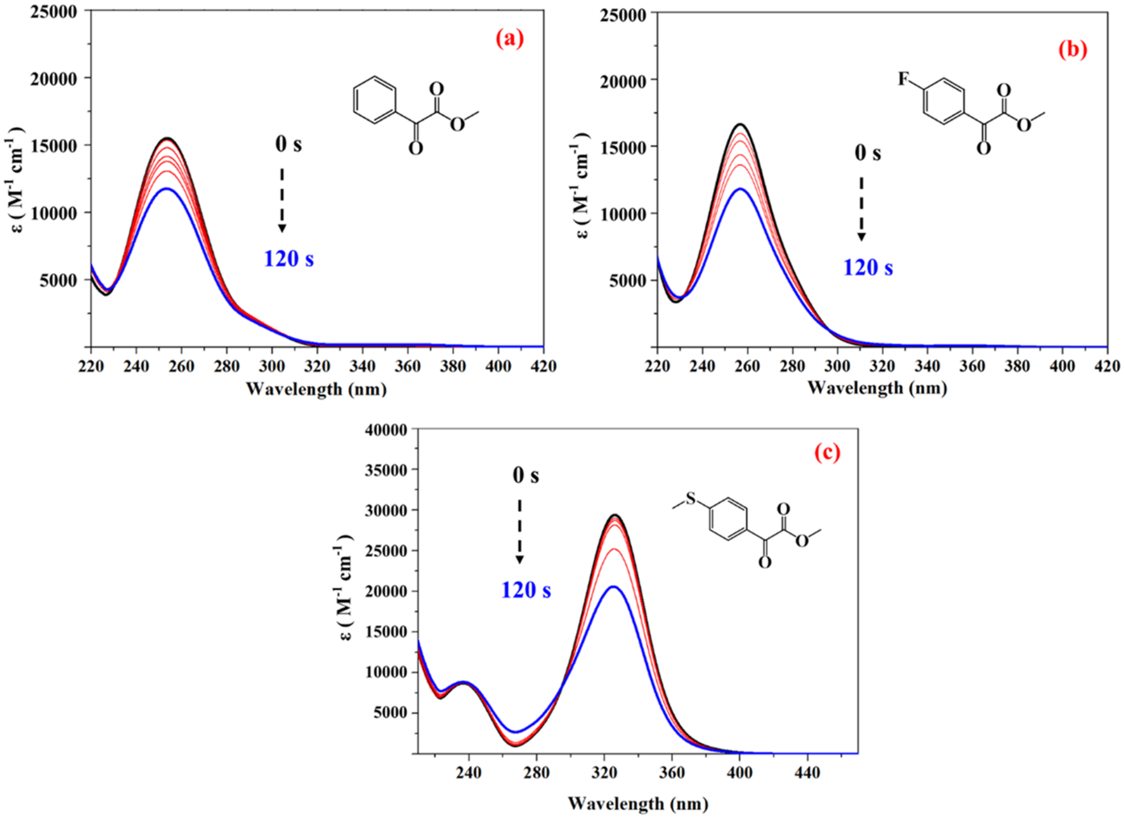

Figure 2. Photolysis curves of (a) MBF, (b) F-MBF, and (c) S-MBF in anhydrous acetonitrile upon LED irradiation at 405 nm (concentration = 1.0×10^{-4} mol L^{-1}).

Scheme 4. Potential Radicals Generated by MBFs

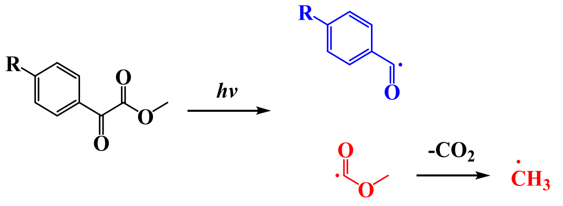

(α_N = 14.00 G, α_H = 5.10 G) were acquired through the literature.[32,37] ESR spectra prove the existence of the substituted benzoyl radical and methyl radical, which further demonstrated that the cleavage reaction of the C−C bond between dicarbonyls and the decarboxylation reaction of the methoxyacyl radical occurred. Extremely similar ESR spectra for all MBFs also mean that MBFs have a similar photolysis mechanism.

In addition, we also tested the ESR spectra of MBF upon exposure to 405 nm LED for different times as shown in Figure S33b to further explore the photolysis behavior of MBFs. The signal intensity gradually increased and simultaneously the shape of the peak also changed with the increase of LED exposure time. It is verified that the ESR signal of MBF for 30 s belongs to benzoyl radicals by comparing with the signal of DB (α_N = 14.2 G, α_H = 5.5 G) as shown in Figure S33a, which implies that benzoyl radicals were dominating radicals in the irradiation system at the initial period of the irradiation.

As depicted in Figure S34, the photodecarboxylation experiment was implemented through bromocresol green pH indicator, which was dissolved in water (left side among two bottles) to detect the carbon dioxide generated by irradiating S-MBF dissolved in acetonitrile (right side among two bottles). The color of the water solution of the indicator changed from blue (neutral) to yellow (acidic) when the acetonitrile solution of S-MBF was continuously irradiated by 405 nm LED, further demonstrating the decarboxylation reaction of the methoxyacyl radical.

ESR experiments and photodecarboxylation experiments both proved the existence of methyl radicals, but we did not find any evidence of the generation of methyl radicals by ^{1}H NMR of the steady-state photolysis products. This phenomenon may be attributed to very few methyl radicals in the system.

In accordance with the above experimental results, we proposed the photolysis mechanism of S-MBF in acetonitrile as shown in Figure 5. The first-step cleavage of the C−C bond between the dicarbonyl happened to generate *p*-methylthiobenzoyl radicals and methoxyacyl radicals. The combination of these two radicals can regenerate S-MBF, 4,4′-dimethylthiobenzyl, or dimethyl oxalate in ACN solvent. In addition, the few methoxyacyl radicals underwent the second-step cleavage (decarboxylation reaction) to generate carbon dioxide and methyl radicals. Substituted benzoyl radicals and methyl radicals possess the capability to initiate photopolymerization.

3.3. Cleavage Exothermy (Δ*H*) for MBFs. The cleavage exothermy (Δ*H*) is a significant and important parameter to evaluate the initiation performances of Norrish type I PIs. It is calculated by this formula: $\Delta H = \mathrm{BDE} - E_E$,[20] where BDE is the bond dissociation energy and E_E refers to the excited-state energy. Generally, the smaller the value of the cleavage exothermy, the better is the photoinitiating performance of PIs.[20]

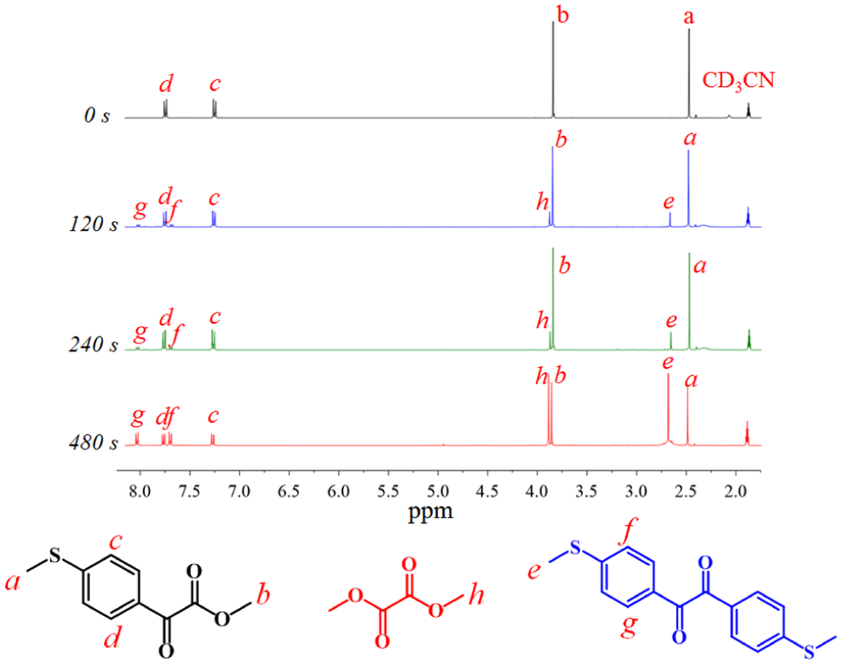

Figure 3. ^{1}H NMR (400 MHz) spectra of the steady-state photolysis products for S-MBF (CD_3CN as the solvent) after LED irradiation at 405 nm for 0, 120, 240, and 480 s, respectively.

As mentioned above, substituted benzoyl radicals generated by the first-step cleavage of MBFs were dominatingly present at the initial period of the irradiation; consequently, only first-step cleavage was considered when calculating the BDE.

It is universally accepted that the cleavage of Norrish type I PIs occurs in triplet state;[29,31,35] therefore, employing the BDE of the triplet state to calculate the ΔH is more reasonable than that of the ground state. Similarly, the triplet-state energy (E_T) was employed to calculate the ΔH.[20] First, we investigated the discrepancy of BDEs between the ground state and triplet state for MBFs by optimizing the molecular conformation of the two states. The optimized geometries of the ground state and triplet state for MBFs are displayed in Figure S35. It is clear that conformations of MBFs have an obvious difference between the ground state and triplet state. The BDEs of the C−C bond between dicarbonyls of MBFs in the ground state and triplet state are calculated based on the optimized geometries of the ground state and triplet state, as shown in Table S3. On the whole, the BDEs of the triplet state (ranging between 150.94 and 108.40 kJ/mol) are much less than those in the ground state (approximately 323 kJ/mol for all MBFs), indicating that the transformation of conformations for MBFs may cause the change of BDE for the C−C bond in dicarbonyls.

Subsequently, the E_T of MBFs was calculated based on the optimized geometries of the ground state and triplet state. The BDE, E_T, and ΔH of MBFs are exhibited in Figure 6, and we can discover that E_T of almost all MBFs is around 220 kJ/mol except for DM-BD-F (246.75 kJ/mol). ΔH of all MBFs is negative, which means that the cleavage reaction is energetically favorable,[20] and all MBFs can initiate the photopolymerization in theory.

In addition, as shown in Figure 6, the photoinitiating capability of MBFs is ranked according to the principle that the lower ΔH is beneficial for PIs to decompose and generate radicals to initiate the polymerization reaction. The first category involving DM-BD-F and TF-MBF may have the most outstanding photoinitiating capability among MBFs because of the smaller ΔH (−127.89 and −111.46 kJ/mol, respectively). The second category involving DF-MBF, F-MBF, Cl-MBF, DC-MBF, O-MBF C-MBF, and MBF, whose ΔH are between −80 and −90 kJ/mol, could have similar initiation performance. The third category involving S-MBF and N-MBF may have the worst capability among investigated MBFs because of the larger ΔH (−68.87 and −72.57 kJ/mol, respectively).

3.4. Photopolymerization under LED Light.

The photopolymerization tests are used to assess the photoinitiating capability of MBFs and verify the accuracy of predicting the photoinitiating capability by computer calculation by employing TPGDA (difunctionality monomer) and TMPTA (trifunctionality monomer).

The photopolymerization kinetics of TPGDA or TMPTA initiated by MBFs and BAPO under LED irradiation at 405 nm are displayed in Figure 7. Obviously, MBFs can initiate the photopolymerization reaction, which is consistent with the calculation result that ΔH of all MBFs is negative. Table S4 lists the double bond conversions of the MBFs/TPGDA system and the BAPO/TPGDA system at 5, 10, 20, and 120 s. Surprisingly, the conversion (70.6%) of the DM-BD-F/TPGDA system at 5 s is close to that (75.3%) of the commercial BAPO/TPGDA and much greater than those (less than 50%) of other MBFs/TPGDA, whereas the double bond conversion of S-MBF/TPGDA and N-MBF/TPGDA at 5 s only reached 1.68 and 7.68%, respectively. Similarly, for MBFs/TMPTA and BAPO/TMPTA systems under LED irradiation at 405 nm, TF-MBF/TMPTA and DM-BD-F/TMPTA exhibit a relatively higher double bond conversion compared with those of other MBFs/TMPTA, while S-MBF/TMPTA and N-MBF/TMPTA present the relatively lower double bond conversion as shown in Figure 7b and Table S5. The findings are consistent with the prediction by the ΔH value, demonstrating that the computer calculation is a very effective means for the molecular design of photoinitiators. In addition, the final double bond conversions of the TMPTA

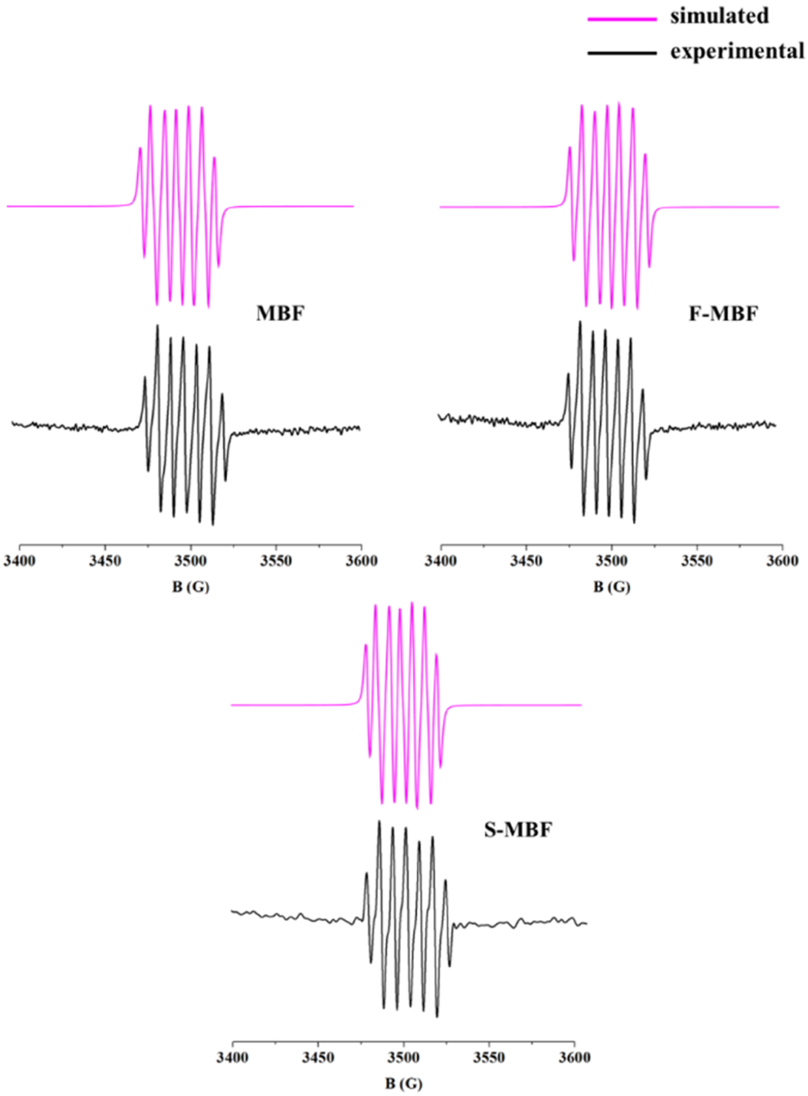

Figure 4. Simulated and experimental ESR spectra of radicals generated by MBF, F-MBF, and S-MBF upon exposure to LED at 405 nm trapped by PBN in *tert*-butylbenzene.

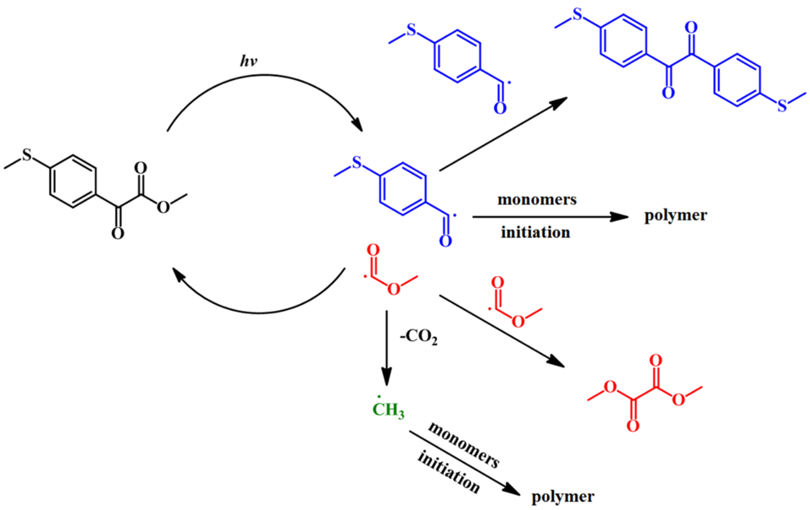

Figure 5. Photolysis mechanism of S-MBF in acetonitrile.

systems are much lower than those of the TPGDA systems, which is related to the viscosity and function of monomers.

Moreover, the above research results also indicate that the electronic effects of substituents on benzene play a decisive

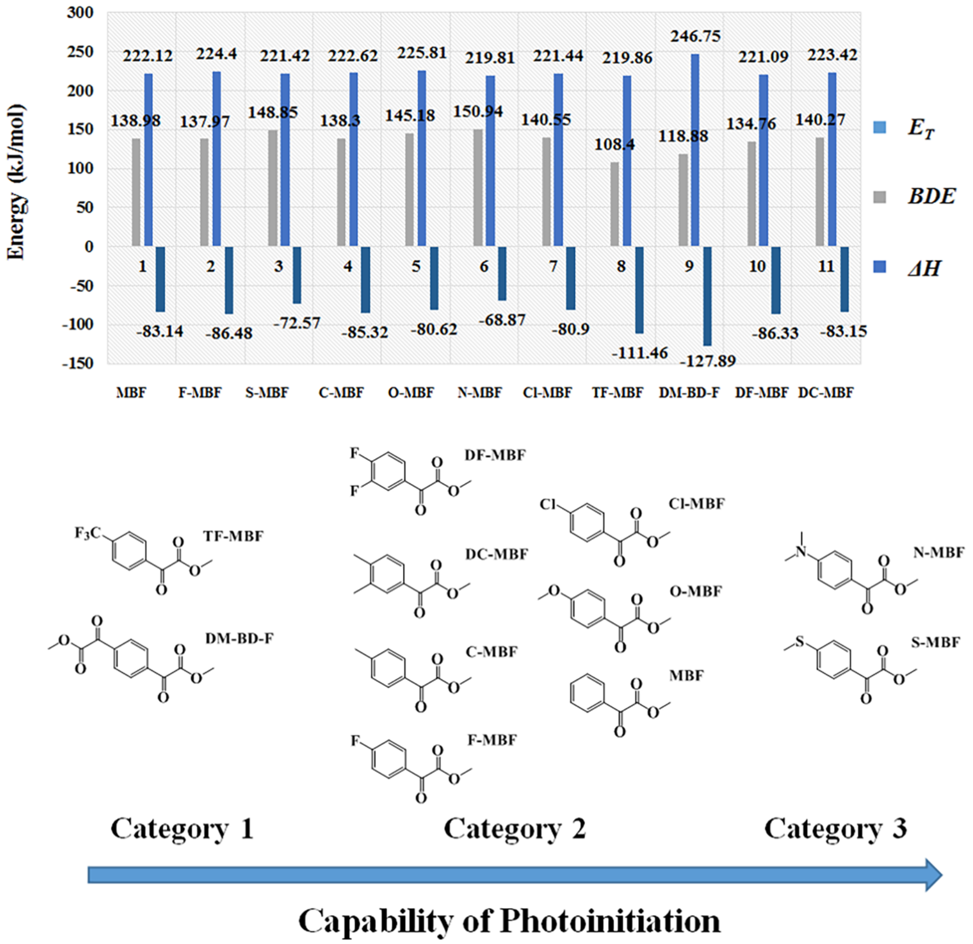

Figure 6. Bond dissociation energy (BDE) in the triplet state, triplet-state energy (E_T), cleavage exothermy (ΔH), and predicted order of the photoinitiating capability according to the value of ΔH of MBFs calculated at B3LYP/6-31G(d).

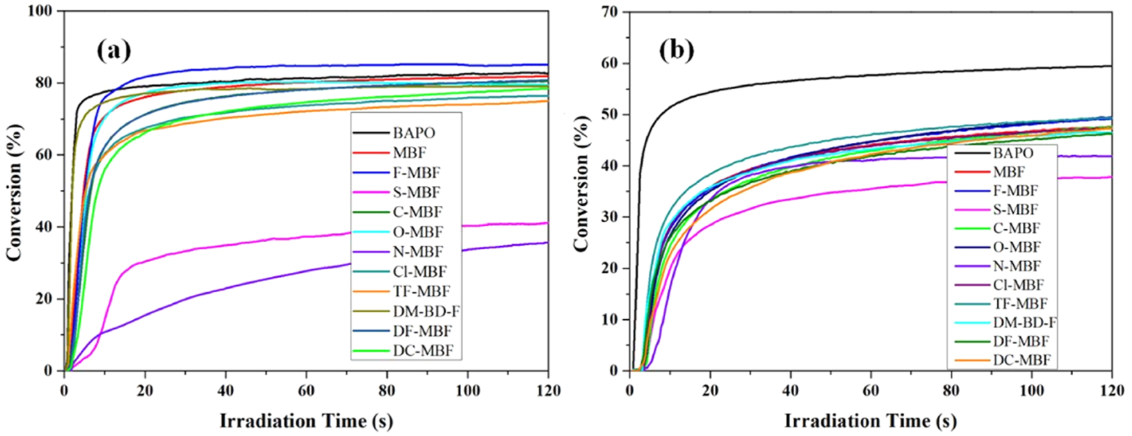

Figure 7. Photopolymerization kinetics of (a) TPGDA and (b) TMPTA in the laminate in the presence of MBFs and BAPO (1 wt %, relative to monomer) upon LED irradiation at 405 nm.

role in the photoinitiating capability of MBFs. The electron-donating substituents such as methylthio (for S-MBF) and dimethylamino (for N-MBF) can weaken the photoinitiating capability of MBFs, whereas electron-withdrawing substituents can improve the photoinitiating capability of MBFs.

3.5. Curing Depth Experiment. The weak absorption in the near-UV and visible-light wavelength range and excellent photoinitiating capability of MBFs are beneficial for deep-layer photocuring. Figure 8 reveals the curing depth experiment under LED irradiation at 405 nm, and the results are shown in Figure 9. Obviously, the curing depth of the BAPO/TPGDA system irradiated by 405 nm LED for 30 s is less than 1.0 cm, while those of the F-MBF/TPGDA, TF-MBF/TPGDA, and DM-BD-F/TPGDA systems reach 5.0 cm, 6.3 cm, and 6.5 cm, respectively, and the cured rods appear colorless, which demonstrates that F-MBF, TF-MBF, and DM-BD-F have a great potential application in fields of LED-induced deep-layer photocuring as well as colorless photocuring materials.

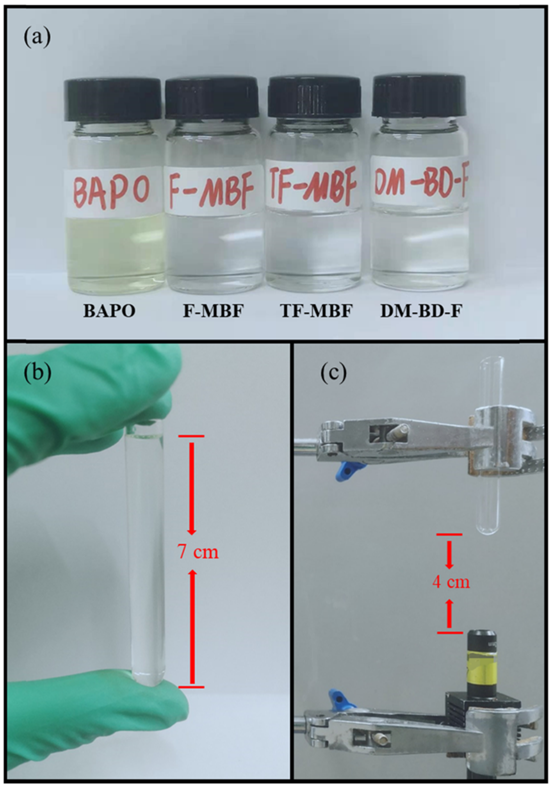

Figure 8. Curing depth experiments for the F-MBF/TPGDA, TF-MBF/TPGDA, DM-BD-F/TPGDA, and BAPO/TPGDA systems (1 wt% for PIs, relative to TPGDA) irradiated by LED at 405 nm for 30 s.

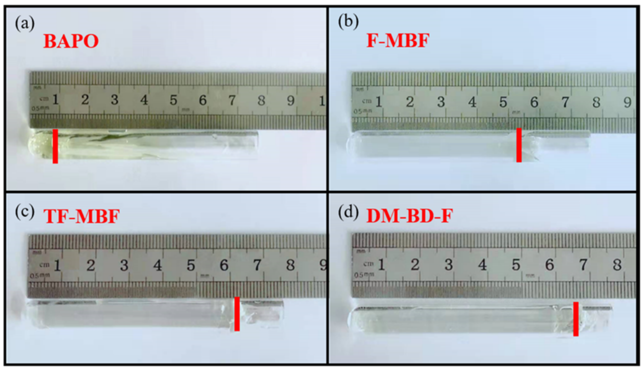

Figure 9. Curing depth experiment results of (a) BAPO/TPGDA, (b) F-MBF/TPGDA, (c) TF-MBF/TPGDA, and (d) DM-BD-F/TPGDA.

4. CONCLUSIONS

Ten MBF photoinitiators for LED-induced photopolymerization have been designed and synthesized. Although the absorption of MBFs in the LED emission wavelength range is very weak, the MBFs still can produce substituted benzoyl radicals and methyl radicals by the first-step cleavage reaction of the C−C bond between dicarbonyls and the second-step decarboxylation reaction, respectively, under a LED irradiation of 405 nm. The substituted benzoyl radicals and methyl radicals can effectively initiate the photopolymerization of acrylate monomers. The electronic effects of substituents on benzene play a key role in the photoinitiating capability of MBFs. DM-BD-F with an electron-withdrawing substituent exhibits excellent photoinitiating capability, which is similar to that of BAPO for TPGDA, while S-MBF and N-MBF with electron-donating substituents show poor photoinitiating capability. Moreover, the photoinitiating capability of MBFs is well predicted through the cleavage exothermy (ΔH) calculated by the triplet bond dissociation energy (BDE) and triplet energy (E_T), which provide an effective strategy for the molecular design of PIs. More importantly, based on the weak absorption of MBFs at 405 nm, MBFs were successfully applied to deep-layer photocuring and the curing depth of the DM-BD-F/TPGDA system reached 6.5 cm and the obtained photocured rods were colorless. MBFs exhibit great potential application for LED-induced deep-layer photocuring as well as colorless photocuring materials. Meanwhile, this research also provides a new idea for the molecular design of photoinitiators for deep-layer photocuring.

■ ASSOCIATED CONTENT

Supporting Information

The Supporting Information is available free of charge at https://pubs.acs.org/doi/10.1021/acs.macromol.0c02868.

> Synthesis route of MBFs and NMR/HRMS data of MBFs; two lowest-energy electronic transitions of S_0−S_1, frontier molecular orbit, transitions type, and energy gap of MBFs; ESR spectra of radicals generated by MBFs upon exposure to LED at 405 nm trapped by PBN in *tert*-butylbenzene; ESR spectra of MBF upon exposure to 405 nm LEDs at 30 s compared with DB upon exposure to 385 nm LEDs at 300 s trapped by PBN in *tert*-butylbenzene and MBF upon exposure to 405 nm LEDs at different times; photodecarboxylation experiment of irradiation at exposure to 405 nm LEDs for S-MBF; optimized geometries of the ground state and triplet state for MBFs; molar extinction coefficients (ε) of MBFs and BAPO in anhydrous acetonitrile at common LED emission wavelengths; two lowest-energy electronic transitions, transition type, and energy gap of MBFs; bond dissociation energy (BDE) in the ground state and triplet state for MBFs; double bond conversion of MBFs/TPGDA, BAPO/TPGDA, MBFs/TMPTA, and BAPO/TMPTA at 5, 10, 20, and 120 s under LED irradiation at 405 nm (PDF)

■ AUTHOR INFORMATION

Corresponding Author

Fang Sun − *State Key Laboratory of Chemical Resource Engineering, Beijing University of Chemical Technology, Beijing 100029, People's Republic of China; College of Chemistry and Anqing Research Institute, Beijing University of Chemical Technology, Beijing 100029, People's Republic of China;* orcid.org/0000-0003-4064-1921;
Email: sunfang60@yeah.net

Authors

Xianglong He − *College of Chemistry, Beijing University of Chemical Technology, Beijing 100029, People's Republic of China;* orcid.org/0000-0002-8352-463X

Yanjing Gao − *College of Chemistry, Beijing University of Chemical Technology, Beijing 100029, People's Republic of China*

Jun Nie − *State Key Laboratory of Chemical Resource Engineering, Beijing University of Chemical Technology,* *Beijing 100029, People's Republic of China; College of Materials Science and Engineering, Beijing University of Chemical Technology, Beijing 100029, People's Republic of China*

Complete contact information is available at:
https://pubs.acs.org/10.1021/acs.macromol.0c02868

Notes

The authors declare no competing financial interest.

■ ACKNOWLEDGMENTS

The financial support from the National Key Research and Development Program of China (2017YFB0307800) and the National Natural Science Foundation of China (Grant No. 52073018) is gratefully acknowledged.

■ REFERENCES

(1) Zhang, J.; Frigoli, M.; Dumur, F.; Xiao, P.; Ronchi, L.; Graff, B.; Morlet-Savary, F.; Fouassier, J. P.; Gigmes, D.; Lalevée, J. Design of Novel Photoinitiators for Radical and Cationic Photopolymerizations under Near UV and Visible LEDs (385, 395, and 405 nm). *Macromolecules* **2014**, *47*, 2811−2819.

(2) Zhang, J.; Launay, K.; Hill, N. S.; Zhu, D.; Cox, N.; Langley, J.; Lalevée, J.; Stenzel, M. H.; Coote, M. L.; Xiao, P. Disubstituted Aminoanthraquinone-Based Photoinitiators for Free Radical Polymerization and Fast 3D Printing under Visible Light. *Macromolecules* **2018**, *51*, 10104−10112.

(3) Chen, S.; Jin, M.; Malval, J.-P.; Fu, J.; Morlet-Savary, F.; Pan, H.; Wan, D. Substituted stilbene-based oxime esters used as highly reactive wavelength-dependent photoinitiators for LED photopolymerization. *Polym. Chem.* **2019**, *10*, 6609−6621.

(4) Sautrot-Ba, P.; Jockusch, S.; Malval, J.-P.; Brezová, V.; Rivard, M.; Abbad-Andaloussi, S.; Blacha-Grzechnik, A.; Versace, D.-L. Quinizarin Derivatives as Photoinitiators for Free-Radical and Cationic Photopolymerizations in the Visible Spectral Range. *Macromolecules* **2020**, *53*, 1129−1141.

(5) Zhang, J.; Lalevee, J.; Hill, N. S.; Peng, X.; Zhu, D.; Kiehl, J.; Morlet-Savary, F.; Stenzel, M. H.; Coote, M. L.; Xiao, P. Photoinitiation Mechanism and Ability of Monoamino-Substituted Anthraquinone Derivatives as Cationic Photoinitiators of Polymerization under LEDs. *Macromol. Rapid Commun.* **2019**, *40*, No. 1900234.

(6) Zhang, J.; Lalevée, J.; Hill, N. S.; Launay, K.; Morlet-Savary, F.; Graff, B.; Stenzel, M. H.; Coote, M. L.; Xiao, P. Disubstituted Aminoanthraquinone-Based Multicolor Photoinitiators: Photoinitiation Mechanism and Ability of Cationic Polymerization under Blue, Green, Yellow, and Red LEDs. *Macromolecules* **2018**, *51*, 8165−8173.

(7) Zhang, J.; Hill, N.; Lalevee, J.; Fouassier, J. P.; Zhao, J.; Graff, B.; Schmidt, T. W.; Kable, S. H.; Stenzel, M. H.; Coote, M. L.; Xiao, P. Multihydroxy-Anthraquinone Derivatives as Free Radical and Cationic Photoinitiators of Various Photopolymerizations under Green LED. *Macromol. Rapid Commun.* **2018**, *39*, No. 1800172.

(8) Peng, X.; Zhu, D.; Xiao, P. Naphthoquinone derivatives: Naturally derived molecules as blue-light-sensitive photoinitiators of photopolymerization. *Eur. Polym. J.* **2020**, *127*, No. 109569.

(9) Xiao, P.; Dumur, F.; Graff, B.; Fouassier, J. P.; Gigmes, D.; Lalevée, J. Cationic and Thiol−Ene Photopolymerization upon Red Lights Using Anthraquinone Derivatives as Photoinitiators. *Macromolecules* **2013**, *46*, 6744−6750.

(10) Eren, T. N.; Graff, B.; Lalevee, J.; Avci, D. Thioxanthone-functionalized 1,6-heptadiene as monomeric photoinitiator. *Prog. Org. Coat.* **2019**, *128*, 148−156.

(11) Karaca, N.; Ocal, N.; Arsu, N.; Jockusch, S. Thioxanthone-benzothiophenes as photoinitiator for free radical polymerization. *J. Photochem. Photobiol., A* **2016**, *331*, 22−28.

(12) Zhang, J.; Dumur, F.; Xiao, P.; Graff, B.; Bardelang, D.; Gigmes, D.; Fouassier, J. P.; Lalevée, J. Structure Design of Naphthalimide Derivatives: Toward Versatile Photoinitiators for Near-UV/Visible LEDs, 3D Printing, and Water-Soluble Photoinitiating Systems. *Macromolecules* **2015**, *48*, 2054−2063.

(13) Yang, J.; Xu, C.; Xiong, Y.; Wang, X.; Xie, Y.; Li, Z.; Tang, H. A Green and Highly Efficient Naphthalimide Visible Photoinitiator with an Ability Initiating Free Radical Polymerization under Air. *Macromol. Chem. Phys.* **2018**, *219*, No. 1800256.

(14) Xiao, P.; Dumur, F.; Zhang, J.; Graff, B.; Gigmes, D.; Fouassier, J. P.; Lalevée, J. New role of aminothiazonaphthalimide derivatives: outstanding photoinitiators for cationic and radical photopolymerizations under visible LEDs. *RSC Adv.* **2016**, *6*, 48684−48693.

(15) Han, W.; Fu, H.; Xue, T.; Liu, T.; Wang, Y.; Wang, T. Facilely prepared blue-green light sensitive curcuminoids with excellent bleaching properties as high performance photosensitizers in cationic and free radical photopolymerization. *Polym. Chem.* **2018**, *9*, 1787−1798.

(16) Zhao, J.; Lalevée, J.; Lu, H.; MacQueen, R.; Kable, S. H.; Schmidt, T. W.; Stenzel, M. H.; Xiao, P. A new role of curcumin: as a multicolor photoinitiator for polymer fabrication under household UV to red LED bulbs. *Polym. Chem.* **2015**, *6*, 5053−5061.

(17) Abdallah, M.; Bui, T.-T.; Goubard, F.; Theodosopoulou, D.; Dumur, F.; Hijazi, A.; Fouassier, J.-P.; Lalevée, J. Phenothiazine derivatives as photoredox catalysts for cationic and radical photosensitive resins for 3D printing technology and photocomposite synthesis. *Polym. Chem.* **2019**, *10*, 6145−6156.

(18) Yang, J.; Xu, C.; Liao, W.; Xiong, Y.; Wang, X.; Tang, H. Visible macrophotoinitiators with Si-H: High efficient anti-oxygen inhibition and modified cured polymer materials. *Prog. Org. Coat.* **2020**, *138*, No. 105410.

(19) Zhou, R.; Sun, X.; Mhanna, R.; Malval, J.-P.; Jin, M.; Pan, H.; Wan, D.; Morlet-Savary, F.; Chaumeil, H.; Joyeux, C. Wavelength-Dependent, Large-Amplitude Photoinitiating Reactivity within a Carbazole-Coumarin Fused Oxime Esters Series. *ACS Appl. Polym. Mater.* **2020**, *2*, 2077−2085.

(20) Dietlin, C.; Trinh, T. T.; Schweizer, S.; Graff, B.; Morlet-Savary, F.; Noirot, P.-A.; Lalevée, J. Rational Design of Acyldiphenylphosphine Oxides as Photoinitiators of Radical Polymerization. *Macromolecules* **2019**, *52*, 7886−7893.

(21) Liu, Y.; Wang, T.; Xie, C.; Tian, X.; Song, L.; Liu, L.; Wang, Z.; Yu, Q. Naphthyl-based acylphosphine oxide photoinitiators with high effiency and low migration. *Prog. Org. Coat.* **2020**, *142*, No. 105603.

(22) Xie, C.; Wang, Z.; Liu, Y.; Song, L.; Liu, L.; Wang, Z.; Yu, Q. A novel acyl phosphine compound as difunctional photoinitiator for free radical polymerization. *Prog. Org. Coat.* **2019**, *135*, 34−40.

(23) Qiu, W.; Li, M.; Yang, Y.; Li, Z.; Dietliker, K. Cleavable coumarin-based oxime esters with terminal heterocyclic moieties: photobleachable initiators for deep photocuring under visible LED light irradiation. *Polym. Chem.* **2020**, *11*, 1356−1363.

(24) Ma, X.; Gu, R.; Yu, L.; Han, W.; Li, J.; Li, X.; Wang, T. Conjugated phenothiazine oxime esters as free radical photoinitiators. *Polym. Chem.* **2017**, *8*, 6134−6142.

(25) Li, Z.; Zou, X.; Zhu, G.; Liu, X.; Liu, R. Coumarin-Based Oxime Esters: Photobleachable and Versatile Unimolecular Initiators for Acrylate and Thiol-Based Click Photopolymerization under Visible Light-Emitting Diode Light Irradiation. *ACS Appl. Mater. Interfaces* **2018**, *10*, 16113−16123.

(26) Ding, Y.; Jiang, S.; Gao, Y.; Nie, J.; Du, H.; Sun, F. Photochromic Polymers Based on Fluorophenyl Oxime Ester Photoinitiators as Photoswitchable Molecules. *Macromolecules* **2020**, *53*, 5701−5710.

(27) Yu, J.; Gao, Y.; Jiang, S.; Sun, F. Naphthalimide Aryl Sulfide Derivative Norrish Type I Photoinitiators with Excellent Stability to Sunlight under Near-UV LED. *Macromolecules* **2019**, *52*, 1707−1717.

(28) Hu, X.; Yu, J.; Jiang, S.; Gao, Y.; Sun, F. Naphthalimide derivatives containing benzyl-sulfur bond as cleavable photoinitiators for near-UV LED polymerization. *J. Sulfur Chem.* **2020**, *41*, 616−634.

(29) Bouzrati-Zerelli, M.; Kirschner, J.; Fik, C. P.; Maier, M.; Dietlin, C.; Morlet-Savary, F.; Fouassier, J. P.; Becht, J.-M.; Klee, J. E.; Lalevée, J. Silyl Glyoxylates as a New Class of High Performance

Photoinitiators: Blue LED Induced Polymerization of Methacrylates in Thin and Thick Films. *Macromolecules* **2017**, *50*, 6911−6923.

(30) Kirschner, J.; Baralle, A.; Graff, B.; Becht, J. M.; Klee, J. E.; Lalevee, J. 1-Aryl-2-(triisopropylsilyl)ethane-1,2-diones: Toward a New Class of Visible Type I Photoinitiators for Free Radical Polymerization of Methacrylates. *Macromol. Rapid Commun.* **2019**, *40*, No. 1900319.

(31) Ma, X.; Cao, D.; Hu, X.; Nie, J.; Wang, T. Carbazolyl α-diketones as novel photoinitiators in photopolymerization under LEDs. *Prog. Org. Coat.* **2020**, *144*, No. 105651.

(32) Pan, H.; Chen, S.; Jin, M.; Malval, J.-P.; Wan, D.; Morlet-Savary, F. A substituentpara-to-orthopositioning effect drives the photoreactivity of a dibenzothiophene-based oxalate series used as LED-excitable free radical photoinitiators. *Polym. Chem.* **2019**, *10*, 1599−1609.

(33) Liao, W.; Xu, C.; Wu, X.; Liao, Q.; Xiong, Y.; Li, Z.; Tang, H. Photobleachable cinnamoyl dyes for radical visible photoinitiators. *Dyes Pigm.* **2020**, *178*, No. 108350.

(34) Mitterbauer, M.; Knaack, P.; Naumov, S.; Markovic, M.; Ovsianikov, A.; Moszner, N.; Liska, R. Acylstannanes: Cleavable and Highly Reactive Photoinitiators for Radical Photopolymerization at Wavelengths above 500 nm with Excellent Photobleaching Behavior. *Angew. Chem., Int. Ed.* **2018**, *57*, 12146−12150.

(35) Fast, D. E.; Lauer, A.; Menzel, J. P.; Kelterer, A.-M.; Gescheidt, G.; Barner-Kowollik, C. Wavelength-Dependent Photochemistry of Oxime Ester Photoinitiators. *Macromolecules* **2017**, *50*, 1815−1823.

(36) Wadhwa, K.; Yang, C.; West, P. R.; Deming, K. C.; Chemburkar, S. R.; Reddy, R. E. Synthesis of Arylglyoxylic Acids and Their Collision-Induced Dissociation. *Synth. Commun.* **2008**, *38*, 4434−4444.

(37) Criqui, A.; Lalevée, J.; Allonas, X.; Fouassier, J.-P. Electron Spin Resonance Spin Trapping Technique: Application to the Cleavage Process of Photoinitiators. *Macromol. Chem. Phys.* **2008**, *209*, 2223−2231.